# Encoding Frequency Constraints in Preventive Unit Commitment Using Deep Learning with Region-of-Interest Active Sampling

Yichen Zhang, Hantao Cui, Jianzhe Liu, Member, IEEE, Feng Qiu, Senior Member, IEEE, Tianqi Hong, Member, IEEE, Rui Yao, Senior Member, IEEE Fangxing (Fran) Li, Fellow, IEEE

Abstract—With the increasing penetration of renewable energy, frequency response and its security are of significant concerns for reliable power system operations. Frequencyconstrained unit commitment (FCUC) is proposed to address this challenge. Despite existing efforts in modeling frequency characteristics in unit commitment (UC), current strategies can only handle oversimplified low-order frequency response models and do not consider wide-range operating conditions. This paper presents a generic data-driven framework for FCUC under high renewable penetration. Deep neural networks (DNNs) are trained to predict the frequency response using real data or highfidelity simulation data. Next, the DNN is reformulated as a set of mixed-integer linear constraints to be incorporated into the ordinary UC formulation. In the data generation phase, all possible power injections are considered, and a region-of-interests active sampling is proposed to include power injection samples with frequency nadirs closer to the UFLC threshold, which significantly enhances the accuracy of frequency constraints in FCUC. The proposed FCUC is verified on the the IEEE 39-bus system. Then, a full-order dynamic model simulation using PSS/E verifies the effectiveness of FCUC in frequency-secure generator commitments.

*Index Terms*—Unit commitment, renewable integration, frequency response, mixed-integer programming, deep learning, active learning.

### NOMENCLATURE

 $i,j, \mathcal{N}_{B}, N_{B}$  index, set, and number of buses

# **Indices and Sets**

index, set, and number of lines
index, set, and number of loads
index, set, number of synchronous generators
index, set, number of wind turbine generators
index, set, number of hidden layers of a neural
network
index, set, number of neurons in a layer
index, set, number of samples
index, set, number of period
Decision Variables
power output of generator $g$ during period $t$
incremental output of generator $g$ from its min-
imum during period $t$
reserve of generator $g$ during period $t$
active, reactive power flow on line $l$ during
period t

 $V_{i,t}$  voltage of bus *i* during period *t* 

# **Discrete Decision Variables**

 $u_{g,t}^{\mathbf{G}}$  1 if unit g is scheduled on during period t and 0 otherwise

#### **Parameters**

$P_{k,t}^{\mathrm{D}}, Q_{k,t}^{\mathrm{D}}$	active, reactive power of load $k$ during period $t$
$P_{k,t}^{\mathrm{D}},  Q_{k,t}^{\mathrm{D}}$ $P_{w,t}^{\mathrm{W}}$	power output of wind turbine generator $\boldsymbol{w}$ during
,	period t
$\underline{P}_l$ , $\overline{P}_l$	min, max active power flow of line $l$
$\underline{Q}_l$ , $\overline{Q}_l$	min, max reactive power flow of line $l$
$\begin{array}{c} \overline{Q}_{l}, \overline{Q}_{l} \\ \underline{P}_{g}^{G}, \overline{P}_{g}^{G} \\ \underline{Q}_{g}^{G}, \overline{Q}_{g}^{G} \\ \underline{V}, \overline{V} \end{array}$	$\min$ , $\max$ active power output of unit $g$
$\underline{Q}_g^{\mathrm{G}},  \overline{Q}_g^{\mathrm{G}}$	$\   \text{min, max reactive power output of unit}g$
$\underline{V}$ , $\overline{V}$	min, max allowable voltages
$\mathbf{W}_m,\mathbf{b}_m$	weight and bias of layer $m$ in a neural network
$\lambda_g^{\rm F}$ $\lambda_g^{\rm M}, \lambda_g^{\rm S}$	fixed cost of unit g at the point of $\underline{P}_q^G$
$\lambda_a^{\rm M}, \lambda_a^{\rm S}$	marginal, start-up cost of unit $g$

#### I. Introduction

With the increasing penetration of renewable energy, power system frequency stability is of significant concern for reliable system operations. The frequency-constrained unit commitment (FCUC) is proposed to address this challenge [1]. The swing equation is used to evaluate the system frequency in [2]. The mechanical output constraints are further taken into account in [3] [4]. Both strategies process a simple constraint set, which is easy to solve. However, important turbine-governor dynamics are not considered. In [5], the dynamics of mechanical power is approximated using an integrator to derive the security criteria of frequency nadir. Ref. [6] employed the formulation in [5] for the interval scheduling problem. In [7] [8], multiple frequency services are considered, where the supported power is approximated by integrator dynamics. Considering the fact that the centerof-inertia (COI) frequency is governed by the classic system frequency response (SFR) model that admits an analytical solution, Refs. [9], [10] derived the analytical expression of the SFR under a step input and proposed an efficient piecewise linearization that converts the analytical solution into a set of constraints. This strategy has been fully extended into microgrid scheduling [11], hierarchical frequency control [12], optimal power flow [13], and unit commitment with renewable energy resources [14], respectively.

Despite these excellent efforts of modeling SFR in mathematical programming-based (MP-based) scheduling, these

methods rely on the low-order model approximation that cannot be able to capture the entire SFR characteristics. In the classic SFR [9] [10], individual generator speeds deviate from the COI frequency depending on the electric distances of generators. Therefore, only considering COI frequency can ignore insecure responses of certain generators. These methods are also unable to incorporate high-order models since there are no analytical solutions for the step response of higher-order differential equations. In addition, nonlinearities in SFR such as deadband and saturation cannot be taken into considerations by the existing approaches, which, however, have significant impacts on SFR [15]. On the other hand, directly incorporating frequency dynamics will result in highly complex MP [16] [17].

To overcome the aforementioned limitations, we propose a deep neural network (DNN)-based trajectory constraint encoding framework to tackle the FCUC. The framework will first train a DNN-based frequency nadir predictor using either real operation data or high-fidelity simulation data. In this case, the frequency nadir predictor can reflect a variety of model types and corresponding nonlinearities. Then, the DNN will be reformulated into a set of mixed-integer linear constraints and further incorporated into the unit commitment program. It is worth mentioning that this re-formulation is exact if the rectified linear unit (ReLU) is employed as the activation function [18].

The main contributions of this paper are concluded as follows: (1) We propose a generic deep learning-based framework for the FCUC. This framework is generic in the sense that it considers the full operation space and can handle all types of differential-algebraic models as well as all possible post-contingency scenarios; (2) We identify the necessary features from the operation variables for training the predictors and derive the mixed-integer linear constraints to encode the feature vectors; (3) We propose a region-of-interest active sampling method to select samples whose frequency nadirs are closer to the UFLS threshold without labeling to generate more informative dataset. We verify that such a method can substantially improve the training efficiency and FCUC accuracy. It is worth mentioning that our previous work [19] only samples over a narrow range of the operating conditions. Though it works for a microgrid, such a sampling strategy is not sufficient for the unit commitment (UC) problems under high renewable penetration, where the operating points can vary significantly from time to time. In this paper, the proposed framework can handle wide-range operation conditions by improving sampling and training efficiency using the regionof-interest active sampling. In addition, the possible unstable trajectories have been taken into account and addressed using an extra stability predictor. Such possible instability has not been considered in the previous FCUC problem.

The remainder of the paper is organized as follows. Section III describes the problem setup. Section III describes the DNN-based predictors for frequency trajectory and stability with feature selections. Section IV describes the data generation using the region-of-interest active sampling strategy. Section V express the FCUC formulation, followed by the case study in Section VI and conclusion in Section VII.

#### II. PROBLEM STATEMENT

The frequency-constrained UC (FCUC) searches the optimal dispatch command such that the resulting system states ensure a secure frequency response for any disturbance from a predefined set  $\mathcal W$  occurring within the scheduling period  $\mathcal T$ . The FCUC reads as follows

$$\min_{\mathbf{u}_t \in \mathcal{U}} C(\mathbf{s}_t, \mathbf{u}_t) \tag{1a}$$

s.t. 
$$\mathbf{f}_{\mathbf{u}}(\mathbf{s}_t, \mathbf{u}_t, \mathbf{d}_t) = 0, \mathbf{g}_{\mathbf{u}}(\mathbf{s}_t, \mathbf{u}_t, \mathbf{d}_t) \le 0$$
 (1b)

$$h^{\mathrm{f}}(\mathbf{s}_t, \mathbf{u}_t, \mathbf{d}_t, \varpi) \ge f_{min}$$
 (1c)

$$h^{\mathbf{p}}(\mathbf{s}_t, \mathbf{u}_t, \mathbf{d}_t, \varpi)_{[2]} \ge h^{\mathbf{p}}(\mathbf{p}_t, \mathbf{u}_t, \mathbf{d}_t, \varpi)_{[1]}$$
 (1d)

$$\forall t \in \mathcal{T}, \varpi \in \mathcal{W} \tag{1e}$$

where  $\mathbf{f}_u$  and  $\mathbf{g}_u$  denotes the equality and inequality constraints, respectively;  $\mathbf{s}_t$  and  $\mathbf{u}_t$  denotes the system states and dispatch variables, respectively. The load forecast is denoted by  $\mathbf{d}$ . The disturbance set  $\mathcal{W}$  is defined to be the N-1 generator loss. Almost, it is guaranteed that the largest generator outage will result in the worst frequency nadir. Thus, we consider the worst-case contingency in the FCUC problem to be the loss of a generator that has the largest power output, which changes with respect to the dispatch signal. The term

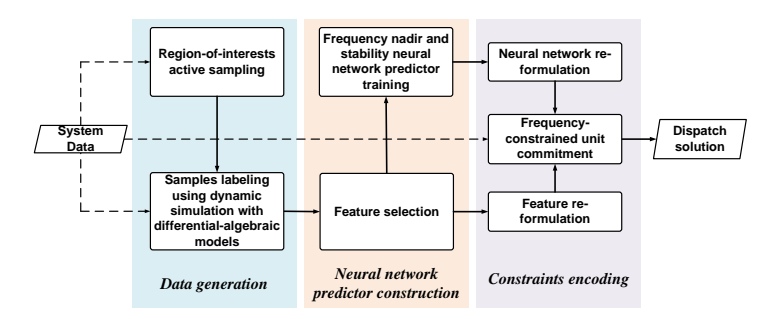


Fig. 1. Overview of the proposed FCUC framework and working pipeline.

 $h^{\rm f}$  is the frequency nadir predictor once the worse-case contingency occurs under the current operating condition. Since we are considering the full power injection space, the network can be subjected to either voltage or rotor angle instability after the worst-case disturbance. The prediction performance can be significantly compromised if these data is incorporated into the training dataset. If not incorporated, however, the frequency nadir predictor may output incorrect values under these unencountered operating condition. The solution is to use a stability predictor  $h^{\rm p}$  that outputs a two-dimensional real-valued vector to filter out the unstable cases as shown in (1d). The first entry denotes the predicted probability of a case being unstable, and the second entry denotes the predicted probability of a case being stable. The subscript [s] denotes the sth entry of the output vector.

# III. DEEP LEARNING-BASED TRAJECTORY CONSTRAINT APPROXIMATION

#### A. DNN-Based Frequency Nadir Predictor

Let this neural network frequency nadir predictor for  $h^f$  be expressed as

$$f_{\text{ndr}} = \hat{h}^{\text{f}}(\mathbf{x}^{\text{f}}; \mathbf{W}^{\text{f}}, \mathbf{b}^{\text{f}}) \tag{2}$$

where  $\mathbf{x}^f$  denotes the feature vector, and  $\mathbf{W}^f$  and  $\mathbf{b}^f$  denote the neural network parameters to be trained. To fully represent all possible operating conditions, a sufficient sample set  $\mathcal{N}_S$  will be created . Let  $f^*_{\text{ndr},s}$  denote the frequency nadir of sample  $\mathbf{x}^f_s$ . Now consider a fully connected neural network with  $N_Y$  hidden layers. Each layer uses a rectified linear unit (ReLU) activation function denoted as  $\sigma(\cdot) = \max(\cdot, 0)$ , and the output layer uses a linear activation function. The predicted nadir can be expressed as follows

$$\mathbf{z}_1^{\mathbf{f}} = \mathbf{x}_s^{\mathbf{f}} \mathbf{W}_1^{\mathbf{f}} + \mathbf{b}_1^{\mathbf{f}} \tag{3a}$$

$$\hat{\mathbf{z}}_{m}^{f} = \mathbf{z}_{m-1}^{f} \mathbf{W}_{m}^{f} + \mathbf{b}_{m}^{f} \tag{3b}$$

$$\mathbf{z}_{m}^{\mathbf{f}} = \max(\hat{\mathbf{z}}_{m}^{\mathbf{f}}, 0) \tag{3c}$$

$$f_{\text{ndr},s} = \mathbf{z}_{N_{\text{v}}}^{\text{f}} \mathbf{W}_{N_{\text{v}}+1}^{\text{f}} + \mathbf{b}_{N_{\text{v}}+1}^{\text{f}}$$
(3d)

where matrix  $\mathbf{W}_i^f$  and vector  $\mathbf{b}_i^f$  for  $i=1,\cdots,N_Y$  represent the set of weight and bias across all hidden layers, and  $\mathbf{W}_{N_Y+1}^f$  and  $\mathbf{b}_{N_Y+1}^f$  represent the set of weight and bias of the output layer. We would like to minimize the total mean squared error between the predicted output and the labeled outputs of all samples using the following

$$\min_{\mathbf{W}_{m}^{f}, \mathbf{b}_{m}^{f}} \frac{1}{N_{S}} \sum_{s=1}^{N_{S}} (f_{\text{ndr},s} - f_{\text{ndr},s}^{*})^{2}$$
 (4)

There are two essential prerequisites: (1) making correct choice of input features among s, u, d and  $\varpi$ ; (2) generating representative samples under different system operating conditions.

1) Feature Selection: The frequency response from a synchronous generator (SG) is less dependent on its output unless there is not enough headroom, which will be avoided in the UC problem. In addition, we assume the droop control of the turbine governor for all SGs will not change. Therefore, it is sufficient to select the status of each SG  $u_{g,s}^{\rm G}$  as the input features. Both the magnitude and location of the disturbance will have impacts on the frequency response. Based on our discussion regarding the disturbance in Section II, the disturbance magnitude can be expressed as

$$P_s^{\varpi} = \max_{g \in \mathcal{N}_G} (P_{1,s}^{G}, \cdots, P_{g,s}^{G}, \cdots, P_{N_{G},s}^{G})$$
 (5)

We use the bus index to represent the location information as

$$g_s^{\varpi} = \arg\max_{g \in \mathcal{N}_{G}} (P_{1,s}^{G}, \cdots, P_{g,s}^{G}, \cdots, P_{N_{G},s}^{G})$$
 (6)

We encode both information into one vector as

$$\mathbf{x}_{s}^{\varpi} = \begin{bmatrix} 0, \cdots, 0 & P_{s}^{\varpi} & 0, \cdots, 0 \\ 0, \cdots, 0 & P_{s}^{\varpi} & 0, \cdots, 0 \end{bmatrix}$$
 (7)

Then, the feature vector of sample s reads as

$$\mathbf{x}_{s}^{\mathbf{f}} = \left[ u_{1,s}^{\mathbf{G}}, \cdots, u_{N_{\mathbf{G}},s}^{\mathbf{G}}, \mathbf{x}_{s}^{\varpi} \right] \tag{8}$$

#### B. DNN-Based Stability Predictor

Similar to the frequency nadir predictor, we construct a neural network  $\hat{h}^p$  to approximate the probabilistic stability descriptor  $h^p$ . To do this, we denote the classes of unstable and stable as  $C_q$  for q=1,2, respectively. The label data after one-hot encoding reads  $\mathbf{e}_s^* = c_{s,1}^*, c_{s,2}^*$ , where  $c_{s,q}^* = 1$  indicates that sample s belongs to class q. We then apply probabilistic smoothing approximations to the discrete label values. It is well known that when the targets are one-hot encoded and an appropriate loss function is used, an neural network directly estimates the posterior probability of class membership  $C_q$  conditioned on the input variables  $\mathbf{x}^p$ , denoted by  $p(C_q|\mathbf{x}^p)$ . Then, the stability predictor can be expressed as follows

$$\mathbf{p}_{\text{stab}} = \left[ p(C_1|\mathbf{x}^p), p(C_2|\mathbf{x}^p) \right] = \hat{h}^p(\mathbf{x}^p; \mathbf{W}^p, \mathbf{b}^p) \quad (9)$$

where  $\hat{h}^p$  reads as follows

$$\mathbf{z}_1^p = \mathbf{x}_s^p \mathbf{W}_1^p + \mathbf{b}_1^p \tag{10a}$$

$$\hat{\mathbf{z}}_m^p = \mathbf{z}_{m-1}^p \mathbf{W}_m^p + \mathbf{b}_m^p \tag{10b}$$

$$\mathbf{z}_{m}^{p} = \max(\hat{\mathbf{z}}_{m}^{p}, 0) \tag{10c}$$

$$\mathbf{p}_{\text{stab},s} = \mathbf{z}_{N_{\mathbf{v}}}^{\mathbf{p}} \mathbf{W}_{N_{\mathbf{v}}+1}^{\mathbf{p}} + \mathbf{b}_{N_{\mathbf{v}}+1}^{\mathbf{p}}$$
(10d)

where  $i=1,\cdots,N_{\rm Y}$  represent the indices for all hidden layers, and  $N_{\rm Y}+1$  is the output layer. The network parameters can be calculated using the maximum likelihood estimation. Therefore, we minimize the negative logarithm of the likelihood function, known as the cross-entropy loss, as follows

$$L = -\frac{1}{N_s} \sum_{s=1}^{N_s} \sum_{q=1}^{2} c_{s,q}^* \log p_s(C_q | \mathbf{x}^p)$$
 (11)

1) Feature Selection: The disturbance information is also essential for the stability predictor. The same encoding method in (5)-(7) is used. Considering that only online SGs will respond to disturbances, their commitment status is also employed. The voltage stability is highly related to the loading condition of the system. Since we relax the generator Var power limits, the active power will have a dominant impact. The transient stability margin depends on the power-angle characteristics, which are determined by the active power injection. Thus, the active power injection of all SGs will be encoded into the feature vector. And the overall feature reads

$$\mathbf{x}_{s}^{p} = [u_{1,s}^{G}, \cdots, u_{N_{G},s}^{G}, \mathbf{x}_{s}^{\varpi}, P_{1,s}^{G}, \cdots, P_{N_{G},s}^{G}]$$
 (12)

# IV. DATA GENERATION AND REGION-OF-INTEREST ACTIVE SAMPLING

Consider a power network with  $N_{\rm G}$  SGs,  $N_{\rm W}$  WTGs, and  $N_{\rm D}$  loads. Let  $\mathcal{N}_{\rm G}$ ,  $\mathcal{N}_{\rm W}$ , and  $\mathcal{N}_{\rm D}$  denote the set of SGs, WTGs and loads, respectively. The full dimension injection samples are

$$\Phi = [\mathbf{P}_{1}^{\mathbf{W}}, \cdots, \mathbf{P}_{N_{\mathbf{W}}}^{\mathbf{W}}, \mathbf{P}_{1}^{\mathbf{G}}, \cdots, \mathbf{P}_{N_{\mathbf{G}}}^{\mathbf{G}}, \mathbf{Q}_{1}^{\mathbf{G}}, \cdots, \mathbf{Q}_{N_{\mathbf{G}}}^{\mathbf{G}}, \mathbf{P}_{N_{\mathbf{G}}}^{\mathbf{D}}, \cdots, \mathbf{P}_{N_{\mathbf{D}}}^{\mathbf{D}}, \mathbf{Q}_{1}^{\mathbf{G}}, \cdots, \mathbf{Q}_{N_{\mathbf{D}}}^{\mathbf{G}}]$$

$$(13)$$

where  $\mathbf{P}_g^{\mathbf{G}}$  and  $\mathbf{Q}_g^{\mathbf{G}}$  are samples of active and reactive power injections for SG g;  $\mathbf{P}_w^{\mathbf{W}}$  are samples of active power injections for WTG w;  $\mathbf{P}_k^{\mathbf{D}}$  and  $\mathbf{Q}_k^{\mathbf{D}}$  are samples of load active and reactive power injections for load k. Each sample in  $\Phi$  is

 $<sup>^1\</sup>mathrm{The}$  subscripts s and t are essentially the same as they both denote different system operating scenarios. Following the convention, we use s in the machine learning problem and t in the UC problem.

denoted as  $\phi_s = \Phi_{[s,:]}^2$ , and the corresponding nadir (label) is denoted as  $f_{\text{ndr},s}$ .

Unlike many works that sample around a narrow operation range, we consider the wide-range space of all power injections in (13) to ensure reliability under vast ranges of operating conditions. In this case, not every sample admits a meaningful frequency nadir. In fact, many sampled power injections are not stable under the worst-case disturbance. Furthermore, what we are concerned about the most is the frequency nadir close to the underfrequency load shedding (UFLS) threshold. Under limited computation resources, it is reasonable to focus on improving the accuracy of frequency nadir prediction near the critical threshold. To train such a predictor, the distribution of the training dataset should contain denser samples where the frequency nadirs are closer to the UFLS threshold, as shown in Fig. 2. To generate such a training set, traditional

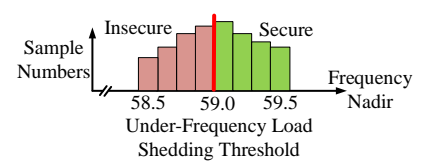


Fig. 2. A conceptual illustration of a desired training dataset.

methods will first perform uniform sampling over all power injections, label all samples to retrieve the nadir information, and then select labeled samples based on desired distributions. However, the labeling procedure needs time-domain simulation with full-order differential-algebraic equations. Labeling adequate samples to achieve desired distributions requires significant computation resources and time, which is known as the *labeling bottleneck*. In other words, *how to sample the power injections whose labels are within the region-of-interest without labeling efforts* is essential.

The proposed active sampling method can proceed as follows. We first define the sample as secure if the corresponding frequency nadir is above the UFLS threshold and insecure otherwise, as illustrated in Fig. 2. Second, we train a frequency security discriminator using the active learning method. The discriminator will output the predicted probability of a sample being secure. Then, we employ the active learning method to train this discriminator. Compared with the traditional passive learning approaches, the active learning method will actively select unlabeled samples, query their labels, and then perform the training on these data instances [20]. During this procedure, samples whose label values are closer to the UFLS are easier to be selected. The rationale lies in the fact that it is more difficult for the discriminator to classify samples that are closer to the decision boundary, which is the UFLS threshold in our case. Therefore, we need to select samples whose posterior probability provided by the discriminator is the closest to 0.5 [20]. In other words, the selected sample is the least confident to the discriminator. Let the frequency security discriminator be denoted as  $Clf(\cdot)$ , the UFLS threshold be denoted as  $f_{\text{UFLS}}$ , the security label of a sample  $\phi_s$  be denoted as  $f_{\text{scr},s}$ , where  $f_{\text{scr},s} = 1$  if  $f_{\text{ndr},s} \geq f_{\text{UFLS}}$  and  $f_{\text{scr},s} = 0$ 

### **Algorithm 1:** Region-of-Interest Active Sampling

```
input: Labeled set \mathcal{L}, unlabeled set \mathcal{U}, sampling
                strategy a(\cdot, \cdot), sampling batch size B, sample
                labeling function Label(\cdot), frequency
                security discriminator Clf(\cdot), discriminator
                training function Train(\cdot, \cdot)
 1 \mathcal{A} \leftarrow \emptyset
                    // initialize the set to store
     acquisition samples
2 repeat
         Clf(\cdot) \leftarrow Train(\mathcal{L}, Clf(\cdot))
                                                         // train the
           discriminator using current {\cal L}
         for s \leftarrow 1 to B do
 4
 5
              \phi_s \leftarrow \arg\max a(\mathcal{U}, \text{Clf}(\cdot))
                sampling using discriminator
              f_{\text{ndr},s}, f_{\text{scr},s} \leftarrow \text{Label}(\phi_s)
 6
              \mathcal{L} \leftarrow \mathcal{L} \cup \langle \phi_s, f_{\text{scr},s} \rangle
 7
              \mathcal{A} \leftarrow \mathcal{A} \cup \langle \phi_s, f_{\text{ndr},s} \rangle
 8
              \mathcal{U} \leftarrow \mathcal{U} - \phi_s
 9
10
         end
11 until some stopping criterion;
    output: All acquisition instances A
```

otherwise. The details of the region-of-interest active sampling algorithm is illustrated in Algorithm 1. The overall strategy is introduced as follows

- 1) Define the frequency security discriminator  $Clf(\cdot)$ ; Among all the samples  $\Phi$ , label a small portion denoted as  $\mathcal{L}$  for frequency security discriminator training
- 2) Initialize the set denoted as  $\mathcal{A}$  to store acquisition samples for frequency nadir predictor training  $\hat{h}_{\mathrm{f}}(\cdot)$
- 3) Train the discriminator using current labeled dataset  $\mathcal L$
- 4) Perform the active sampling using the discriminator; The active sampling function  $a(\mathcal{U}, Clf(\cdot))$  reads as follows

$$\phi_s = \underset{\mathcal{U}}{\operatorname{argmax}} a(\mathcal{U}, \operatorname{Clf}(\cdot))$$

$$= \underset{\mathcal{U}}{\operatorname{argmax}} \left( -\sum_{i=0}^{1} p(i|\mathcal{U}) \log p(i|\mathcal{U}) \right)$$
(14)

where  $p(i|\mathcal{U})$  is the predicted posterior probability of class membership (0 for insecure and 1 for secure) conditioned on the sample inputs.

- 5) Retrieve both nadir and security labels; Add the nadir label  $f_{\text{ndr},s}$  with the acquired sample  $\phi_s$  to  $\mathcal{A}$ ; Add the security label  $f_{\text{scr},s}$  with the acquired sample  $\phi_s$  to  $\mathcal{L}$ ; Remove the sample from the unlabeled pool.
- 6) Repeat (4) and (5) to reach the batch number; Repeat (3)-(5) for the entire process

It is worth mentioning that the ultimate goal of Algorithm 1 is to generate the dataset  $\mathcal{A}$  for training the frequency nadir predictor  $\hat{h}_{\rm f}$ . By calculating the entropy of the security discriminator outputs and selecting the extreme value, the corresponding samples will be closer to the decision boundary, that is, the UFLS threshold.

<sup>&</sup>lt;sup>2</sup>The subscript [s,:] denotes the sth row of a matrix.

#### V. FREQUENCY CONSTRAINED UNIT COMMITMENT

In this section, we will introduce the FCUC formulation. Consider an  $N_B$ -bus power network. Let  $\sigma_q(\cdot)$ ,  $\sigma_w(\cdot)$  and  $\sigma_d(\cdot)$ map from the bus index i to the device index g, w, k that is connected to bus i. Consider the scheduling period from 1 to  $N_{\rm T}$ . Each SG should be dispatched with the permissible limits

$$0 \le p_{q,t}^{G} \le (\overline{P}_{q}^{G} - \underline{P}_{q}^{G})u_{q,t}^{G} \quad \forall g$$
 (15a)

$$\underline{Q}_{g}^{\mathrm{G}}u_{g,t}^{\mathrm{G}} \leq Q_{g,t}^{\mathrm{G}} \leq \overline{Q}_{g}^{\mathrm{G}}u_{g,t}^{\mathrm{G}} \quad \forall g \tag{15b}$$

$$P_{g,t}^{G} = p_{g,t}^{G} + \underline{P}_{g}^{G} u_{g,t}^{G} \quad \forall g$$
 (15c)

$$t = 1, \cdots, N_{\rm T} \tag{15d}$$

The dispatch changes should respect the ramp-up and rampdown limits

$$\begin{split} P_{g,t}^{\rm G} - P_{g,t-1}^{\rm G} &\leq \overline{R}_g^{\rm G} u_{g,t-1}^{\rm G} + \underline{P}_g^{\rm G} (u_{g,t}^{\rm G} - u_{g,t-1}^{\rm G}) \forall g \\ P_{g,t-1}^{\rm G} - P_{g,t}^{\rm G} &\leq \underline{R}_g^{\rm G} u_{g,t-1}^{\rm G} + \underline{P}_g^{\rm G} (u_{g,t-1}^{\rm G} - u_{g,t}^{\rm G}) \forall g \end{split} \tag{16a}$$

$$P_{g,t-1}^{G} - P_{g,t}^{G} \le \underline{R}_{g}^{G} u_{g,t-1}^{G} + \underline{P}_{g}^{G} (u_{g,t-1}^{G} - u_{g,t}^{G}) \forall g$$
 (16b)

$$t = 2, \cdots, N_{\rm T} \tag{16c}$$

The commitment commands should meet the minimum-up and -down time constraints

$$u_{a,t}^{G} - u_{a,t-1}^{G} \le u_{a,\tau^{up}}^{G} \quad \forall g \tag{17a}$$

$$u_{g,t}^{G} - u_{g,t-1}^{G} \le u_{g,\tau^{up}}^{G} \quad \forall g$$
 (17a)  
 $u_{g,t-1}^{G} - u_{g,t}^{G} \le 1 - u_{g,\tau^{down}}^{G} \quad \forall g$  (17b)

$$t = 2, \cdots, N_{\rm T} \tag{17c}$$

$$\tau^{\text{up}} = t + 1, \cdots, \min(t + t_q^{\text{up}} - 1, N_{\text{T}})$$
 (17d)

$$\tau^{\text{down}} = t + 1, \cdots, \min(t + t_a^{\text{down}} - 1, N_{\text{T}})$$
 (17e)

And for t = 1, the minimum-up and -down time constraints read as follow

$$u_{g,1}^{\mathrm{G}} \leq u_{g,\tau^{\mathrm{up}}}^{\mathrm{G}} \quad \forall g \tag{18a} \label{eq:18a}$$

$$u_{g,1}^{\mathbf{G}} \le 1 - u_{g,\tau^{\mathrm{down}}}^{\mathbf{G}} \quad \forall g$$
 (18b)

$$\tau^{\text{up}} = 2, \cdots, \min(t + t_q^{\text{up}} - 1, N_{\text{T}})$$
(18c)

$$\tau^{\text{down}} = 2, \cdots, \min(t + t_g^{\text{down}} - 1, N_{\text{T}})$$
(18d)

The linearized AC power flow equations and the voltage constraints are expressed as follows

$$P_i^{\text{inj}} = G_{ij}(2V_{i,t} - 1) - G_{ij}(V_{i,t} + V_{j,t} - 1) - B_{ij}(\theta_{i,t} - \theta_{i,t}) \quad \forall i, j, i \neq j, \forall t$$
(19a)

$$Q_{i}^{\text{inj}} = B_{ij}(1 - 2V_{i,t} + B_{ij}(V_{i,t} + V_{j,t} - 1) - G_{ij}(\theta_{i,t} - \theta_{j,t}) \quad \forall i, j, i \neq j, \forall t$$
(19b)

$$\underline{V} \le V_{i,t} \le \overline{V} \quad \forall i, \forall t \tag{19c}$$

where

$$P_i^{\text{inj}} = \sum_{g \in \sigma_g(i)} P_g^{\text{G}} + \sum_{w \in \sigma_w(i)} P_w^{\text{W}} - \sum_{k \in \sigma_d(i)} P_k^{\text{D}} \quad \forall i \quad (20a)$$

$$\begin{split} P_i^{\text{inj}} &= \sum_{g \in \sigma_g(i)} P_g^{\text{G}} + \sum_{w \in \sigma_w(i)} P_w^{\text{W}} - \sum_{k \in \sigma_d(i)} P_k^{\text{D}} \quad \forall i \quad \text{(20a)} \\ Q_i^{\text{inj}} &= \sum_{g \in \sigma_g(i)} Q_g^{\text{G}} - \sum_{k \in \sigma_d(i)} Q_k^{\text{D}} \quad \forall i \quad \text{(20b)} \end{split}$$

To encode the DNN into the MILP, we will first build the feature vectors in terms of the decision variables in the UC problem. Then, we will express the trained neural networks as MILP models. As discussed before, we replace the sample

index with the scheduling period index. The feature vectors for the frequency nadir and stability predictors defined in terms of the decision variables are expressed in (8) and (12), respectively. Unfortunately,  $\mathbf{x}_{t}^{\varpi}$  contains the max operator, and  $\mathbf{x}_t^{\mathrm{f}}$  and  $\mathbf{x}_t^{\mathrm{p}}$  cannot be directly used in the encoding formulation. Thus, we introduce the supplementary variables  $\nu_{a,t}^{G}$  to indicate if generator g outputs the largest active power in scheduling period t. The re-formulations are expressed as follows

$$P_{\varrho,t}^{\mathbf{G}} - P_{g,t}^{\mathbf{G}} \le M(1 - \nu_{g,t}^{\mathbf{G}}) \quad \forall \varrho, g \in \mathcal{N}_{\mathbf{G}}, \forall t$$
 (21a)

$$\sum_{g \in \mathcal{N}_G} \nu_{g,t}^{\mathbf{G}} = 1 \forall t \tag{21b}$$

where M is a big number. Eq. (21a) enforces  $\nu_{q,t}^{G}$  to be zero if the output of any generators  $\varrho$  is greater than g during period t. Eq. (21b) ensures that there should be only one largest generator during t. The combination of both constraints will ensure generator g has the largest output if  $\nu_{q,t}^{G} = 1$ . To further encode the magnitude information, we define another supplementary variables  $\vartheta^\varpi_{g,t}$  and let  $\vartheta^\varpi_{g,t}=P^{\rm G}_{g,t}$  if  $\nu^{\rm G}_{g,t}=1$ , and  $\vartheta^\varpi_{g,t}=0$  otherwise. The corresponding constraints are

$$\vartheta_{q,t}^{\varpi} - P_{q,t}^{G} \ge -M(1 - \nu_{q,t}^{G}) \quad \forall g \in \mathcal{N}_{G}, \forall t$$
 (22a)

$$\vartheta_{q,t}^{\varpi} - P_{q,t}^{G} \le M(1 - \nu_{q,t}^{G}) \quad \forall g \in \mathcal{N}_{G}, \forall t$$
 (22b)

$$0 \le \vartheta_{q,t}^{\varpi} \le M \nu_{q,t}^{G} \quad \forall g \in \mathcal{N}_{G}, \forall t$$
 (22c)

Finally, the feature vector for frequency nadir prediction can be re-written as follows

$$\mathbf{x}_{t}^{\mathbf{f}} = \left[ u_{1,t}^{\mathbf{G}}, \cdots, u_{N_{\mathbf{G}},t}^{\mathbf{G}}, \vartheta_{1,t}^{\varpi}, \cdots, \vartheta_{N_{\mathbf{G}},t}^{\varpi} \right]$$
 (23)

And the feature vector for stability prediction can be re-written

$$\mathbf{x}_{t}^{\mathsf{p}} = \left[u_{1,t}^{\mathsf{G}}, \cdots, u_{N_{\mathsf{G}},t}^{\mathsf{G}}, \vartheta_{1,t}^{\varpi}, \cdots, \vartheta_{N_{\mathsf{G}},t}^{\varpi}, P_{1,t}^{\mathsf{G}}, \cdots, P_{N_{\mathsf{G}},t}^{\mathsf{G}}\right] \tag{24}$$

Then, we can express the trained frequency nadir predictor  $\hat{h}^{\rm f}$  in (3) and stability predictor  $\hat{h}^{\rm p}$  in (10) as MILP models to encode the predictions of decision variables and indirectly impose frequency security and stability constraints on decision variables. Since most parts of the model are similar, we use the superscript  $\alpha$  to denote the types of the neural networks, where  $\alpha \in \{f, p\}$ . The MILP formulations read as follows

$$\mathbf{z}_{1\,t}^{\alpha} = \mathbf{x}_{t}^{\alpha} \mathbf{W}_{1}^{\alpha} + \mathbf{b}_{1}^{\alpha} \quad \forall t \tag{25a}$$

$$\hat{\mathbf{z}}_{m\,t}^{\alpha} = \mathbf{z}_{m-1\,t}^{\alpha} \mathbf{W}_{m}^{\alpha} + \mathbf{b}_{m}^{\alpha} \quad \forall m, \forall n, \forall t$$
 (25b)

$$\mathbf{z}_{m[n],t}^{\alpha} \leq \hat{\mathbf{z}}_{m[n],t}^{\alpha} - \underline{\mathbf{h}}_{m[n]}^{\alpha} (1 - \mathbf{a}_{m[n],t}^{\alpha}) \quad \forall m, \forall n, \forall t \quad (25c)$$

$$\mathbf{z}_{m[n],t}^{\alpha} \ge \hat{\mathbf{z}}_{m[n],t}^{\alpha} \quad \forall m, \forall n, \forall t$$
 (25d)

$$\mathbf{z}_{m[n],t}^{\alpha} \le \overline{\mathbf{h}}_{m[n]}^{\alpha} \mathbf{a}_{m[n],t}^{\alpha} \quad \forall m, \forall n, \forall t$$
 (25e)

$$\mathbf{z}_{m[n]\ t}^{\alpha} \ge 0 \quad \forall m, \forall n, \forall t \tag{25f}$$

$$\mathbf{a}_{m,t}^{\alpha} \in \{0,1\}, \alpha \in \{f, p\} \tag{25g}$$

$$f_{\text{ndr},t} = \mathbf{z}_{N_{\text{Y}},t}^{\text{f}} \mathbf{W}_{N_{\text{Y}}+1}^{\text{f}} + \mathbf{b}_{N_{\text{Y}}+1}^{\text{f}} \quad \forall t$$
 (25h)

$$\mathbf{p}_{\text{stab},t} = \mathbf{z}_{N_{\text{Y}},t}^{\text{p}} \mathbf{W}_{N_{\text{Y}}+1}^{\text{p}} + \mathbf{b}_{N_{\text{Y}}+1}^{\text{p}} \quad \forall t$$
 (25i)

As shown, except for the final layers in (25h) and (25i), the rest parts of the neural networks admit the same reformulations for both  $\hat{h}^f$  and  $\hat{h}^p$ . A binary vector  $\mathbf{a}_m^{\alpha}$  for  $\alpha \in \{\mathrm{f},\mathrm{p}\}$  represents the activation status of ReLU at mth hidden layer, and  $\mathbf{a}_{m[n]}^{\alpha}$  represents the status of the nth neuron at the mth layer. Let  $[\underline{\mathbf{h}}_{m[n]}^{\alpha},\overline{\mathbf{h}}_{m[n]}^{\alpha}]$  be an interval that is large enough to contain all possible values of  $\hat{\mathbf{z}}_{m[n]}^{\alpha}$ , where  $\underline{\mathbf{h}}_{m[n]}^{\alpha} < 0$  and  $\overline{\mathbf{h}}_{m[n]}^{\alpha} > 0$ . When  $\hat{\mathbf{z}}_{m[n]}^{\alpha}$  is less than or equal to zero, constraints (25c) and (25f) will force  $\mathbf{a}_{m[n]}^{\alpha}$  to be zero. In this case, constraints (25e) and (25f) imply that  $\mathbf{z}_{i[k]}^{\alpha} = 0$ , so we have  $\hat{\mathbf{z}}_{m[n]}^{\alpha} \leq 0 \implies \mathbf{a}_{m[n]}^{\alpha} = 0 \implies \hat{\mathbf{z}}_{m[n]}^{\alpha} = 0$ . When  $\hat{\mathbf{z}}_{m[n]}^{\alpha}$  is greater than zero, constraints (25c) and (25f) will force  $\mathbf{a}_{m[n]}^{\alpha}$  to be 1. In this case, constraints (25c) and (25d) imply that  $\mathbf{z}_{m[n]}^{\alpha} = \hat{\mathbf{z}}_{m[n]}^{\alpha}$ , so we have  $\hat{\mathbf{z}}_{m[n]}^{\alpha} > 0 \implies \mathbf{a}_{m[n]}^{\alpha} = 1 \implies \mathbf{z}_{m[n]}^{\alpha} = \hat{\mathbf{z}}_{m[n]}^{\alpha}$ . Obviously, this formulation contains no approximation of the original model. In addition, this is the tightest possible formulation with respect to its LP relaxation if no future information about  $\hat{\mathbf{z}}_{m[n]}^{\alpha}$  is revealed [18].

Finally, we impose the frequency security constraint and stability constraint on the predictions

$$f_{\text{ndr},t} \ge f_{\text{UFLS}} \quad \forall t$$
 (26a)

$$(\mathbf{p}_{\mathrm{stab},t})_{[2]} \ge (\mathbf{p}_{\mathrm{stab},t})_{[1]} + \varepsilon_{\mathrm{stab},t} \quad \forall t$$
 (26b)

where  $\varepsilon_{\mathrm{stab},t}$  is the supplementary variable to relax the predicted stability condition. Since only the steady-state information is used for dynamic stability prediction, the accuracy is relatively low. Therefore, strictly enforcing the predicted stability condition requires significant searches for feasible solutions and is not computationally efficient. Essentially, the stability predictor tries to filter out as many samples as possible that are not encountered by the frequency nadir predictor. The relaxed formulation can sufficiently minimize this risk.

The two-segment cost function, consisting of the fixed and marginal costs, is employed. The scheduling objective is to minimize the total operational cost, expressed as follows

min 
$$\sum_{t=1}^{N_{\rm T}} \sum_{g=1}^{N_{\rm G}} \left[ \lambda_g^{\rm M} p_{g,t}^{\rm G} + \lambda_g^{\rm F} u_{g,t}^{\rm G} \right]$$
 (27a)

$$+\sum_{t=2}^{N_{\rm T}-1}\sum_{g=1}^{N_{\rm G}}\lambda_g^{\rm S}w_{g,t}^{\rm G}$$
 (27b)

$$+\sum_{t=1}^{N_{\rm T}} \Gamma \varepsilon_{{\rm stab},t} \tag{27c}$$

where  $p_{g,t}^{\rm G}$  denotes the incremental outputs of SG g,  $\lambda^{\rm F}$  and  $\lambda^{\rm M}$  denote the fixed and marginal costs, respectively. Terms (27a) and (27b) represent the fuel and start-up costs of SGs, respectively. Terms (27c) represents the stability risk with a weighting factor  $\Gamma$ . It is worth noting that reformulation of the start-up cost has already been carried out in (27b), where  $w_{g,t}^{\rm G}$  is the slack binary variable. In addition,  $w_{g,t}^{\rm G}$  and  $u_{g,t}^{\rm G}$  are subject to the following constraints

$$w_{g,t}^{\text{G}} \ge 0, w_{g,t}^{\text{G}} \ge u_{g,t}^{\text{G}} - u_{g,t-1}^{\text{G}} \quad \forall g, t = 2, \cdots, N_{\text{T}}$$
 (28)

# VI. CASE STUDY

We use the IEEE 39-bus system to demonstrate the framework. The PSS/E software has been widely used in the power industry for dynamic security assessment in daily operations, and thus is chosen for labeling the samples. We use full-scale models for the dynamic simulation during the labeling process: GENTPJU1 for the synchronous machine; IEEEX1 for the excitation system; IEESGO for the turbine-governor; PSS2A for the power system stabilizer. We assume there are four WTGs installed at Buses 2, 10, 20, 25, respectively. Each WTG is an equivalent representation of 600 1.5MW realistic Type-3 WTGs. Standard WTG and corresponding control modules are employed: WT3G2 for the doubly-fed induction machine, WT3E1 for the electric control, WT3T1 for the mechanical model, WT3P1 for the pitch control. Details of these models can be found in [21]. The forecast aggregated load and wind power are plotted in Fig. 3. The aggregated load is distributed to each bus based on the ratio of demand in the power flow data.

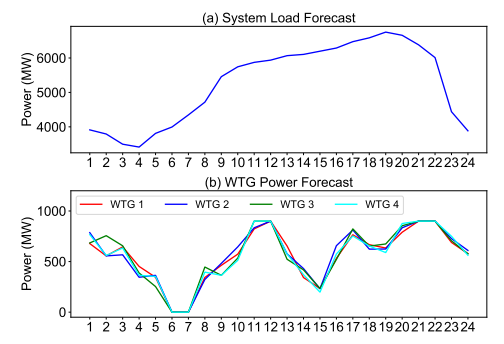


Fig. 3. (a) System load forecast. (b) WTG power forecast.

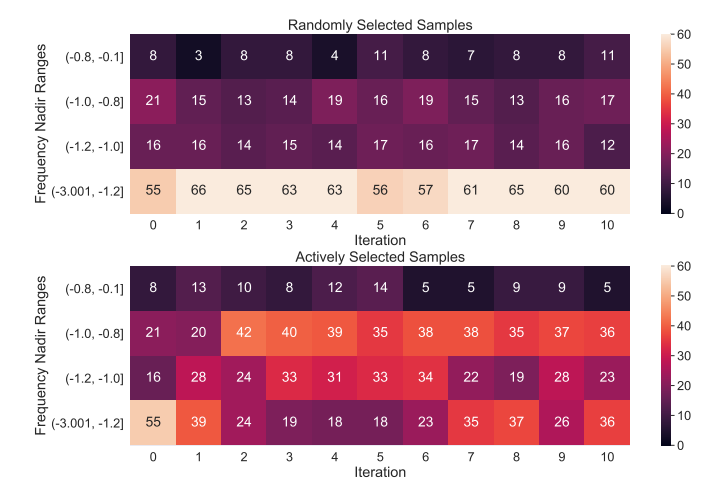


Fig. 4. Samples selected by active and random strategies. The number in each box represents how many samples whose label values are within the interval are selected in this iteration. The active method selects more samples within the region of interest, that is, close to the UFLS threshold.

#### A. Region-of-Interest Active Sampling and DNN Training

We first generate 5000 power injection samples as described in (13) with negligible computation efforts. For generators, the active power injections are uniformly sampled over the lower and upper bounds. We assume SGs have adequate reactive power capacity, and WTGs are controlled with unity power factor. Therefore, we do not need to sample the reactive power of all generators. For loads, both active and reactive power

are sampled based on the Gaussian distribution. The means are equal to the demand values in the power flow data, and deviations are equal to 30% of their nominal values.

With all these unlabeled samples, we employ the activelyselect-then-label strategy described in Section IV to generate the training dataset. For comparison, another dataset is generated using the randomly-select-then-label procedure. In each iteration, 100 samples will be selected for PSS/E to label. We divide the nadir values of frequency deviation into four intervals: [-3, -1.2], [-1.2, -1.0], [-1.0, -0.8], [-0.8, -0.1]. The regions of interest are [-1.2, -1.0] and [-1.0, -0.8] since they are closer to the UFLS threshold. The heatmap of the selected samples with both active and random methods are shown in Fig. 4. The number in each box represents how many samples whose label values are within the interval are selected in this iteration. As shown, the active method selects more samples within the region of interest. In addition, if we use random sampling, more than 50% of the samples are unstable and not available for frequency nadir predictor training. This number will reduce to around 25% if the active sampling strategy is employed, and thus greatly improve the labeling efficiency.

We use *actively-select-then-label* and *randomly-select-then-label* strategies to train two frequency nadir predictor, respectively. For the validation, we first generate another 5000 randomly selected samples. Then, we label the validation dataset and select those with label values greater than -1.2. The following metrics are used to demonstrate the prediction accuracy: (1) maximum error (MAX-E), (2) median absolute error (MED-E), (3) mean absolute error (MEA-E), and (4)  $R^2$  score, which is defined as follows

$$R^{2}(f_{\text{ndr},s}, f_{\text{ndr},s}^{*}) = 1 - \frac{\sum_{s=1}^{N_{s}} (f_{\text{ndr},s}^{*} - f_{\text{ndr},s})^{2}}{\sum_{s=1}^{N_{s}} (f_{\text{ndr},s}^{*} - \overline{f}_{\text{ndr}}^{*})^{2}}$$
(29)

 $R^2$  score gives some information about the goodness of model fitting. In regression, the  $R^2$  coefficient of determination is a statistical measure of how well the regression predictions approximate the real data points. An  $R^2$  of 1 indicates that the regression predictions perfectly fit the data. The validation results of the predictors trained using actively and randomly selected samples are shown in Table I. This result verifies the data generation strategy in Section IV, that is, a training dataset with the distribution shown in Fig. 2 and lower figure in Fig. 4 will improve the accuracy.

TABLE I VALIDATION OF PREDICTORS TRAINED USING ACTIVELY AND RANDOMLY SELECTED SAMPLES

Case	MAX-E	MED-E	MEA-E	$R^2$
Active	0.3539	0.0225	0.0281	0.9352
Random	0.4511	0.0298	0.0376	0.8782

#### B. FCUC Results

The voltages are allowed to variate between 0.8 and 1.2 p.u. The unit commitment results of ordinary formulations (Eqs. (15)-(19)) and (27) are shown in Fig. 5. While, the

results of FCUC formulations (Eqs. (15)-(27)) are shown in Fig. 6, where the frequency security limit is set to be 59 Hz. A stability predictor with 78% accuracy is trained and incorporated. As we can see, FCUC formulation enforces more SGs to be committed such that adequate responsive active and reactive power is online to ensure both stability and dynamic frequency security. The FCUC also makes the outputs of different SGs to be more equalized to reduce the risk of stability and security under the worst-case contingency. Particularly, the system under ordinary dispatch strategy is vulnerable to the N-1 generator outage event during nights. These are periods when the wind power is abundant, and demand is deficient, resulting in less committed SGs. For example, in the scheduling periods 23 and 24, ordinary UC only schedules four SGs shown in Fig. 5. In contrast, FCUC formulation commits seven SGs illustrated in Fig. 6.

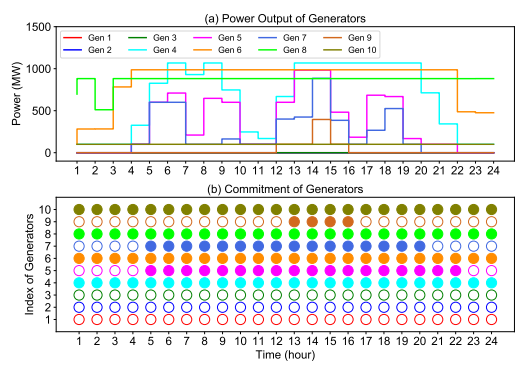


Fig. 5. UC results using ordinary formulations. (a) Power outputs of SGs. (b) Commitment of SGs.

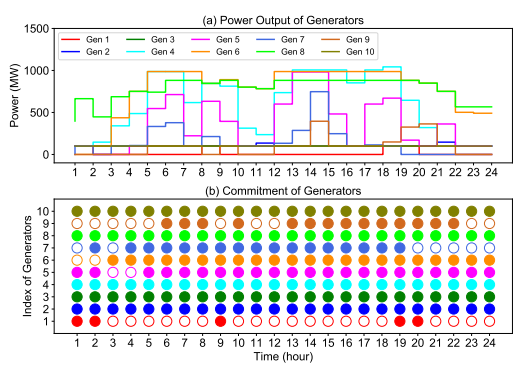


Fig. 6. UC results with frequency trajectory constraints. (a) Power outputs of SGs. (b) Commitment of SGs.

We assume the worst-case contingency takes place in the period 24, and the generator outputting the largest power is tripped. The system under the ordinary UC schedules does not have a power flow solution after the disturbance. While, the system frequency responses following the FCUC dispatch are shown in Fig. 7, which satisfy the frequency trajectory constraint. The voltage dynamics and active power outputs of generators are plotted in Fig. 8 (a) and (b), respectively. Fig. 8 (a) indicates that the FCUC dispatch also satisfy the voltage limits. Fig. 8 (b) illustrates the generator tripping and responses from other generators except for the WTGs.

The systematic verification using PSS/E is shown in Table II. The first column is the predicted deviated frequency nadir

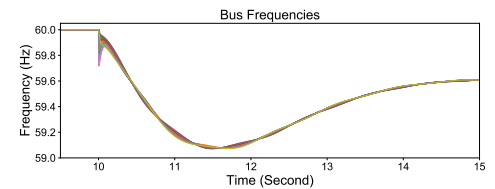


Fig. 7. Frequency response under the FCUC dispatch and worst-case contingency during the scheduling period 24.

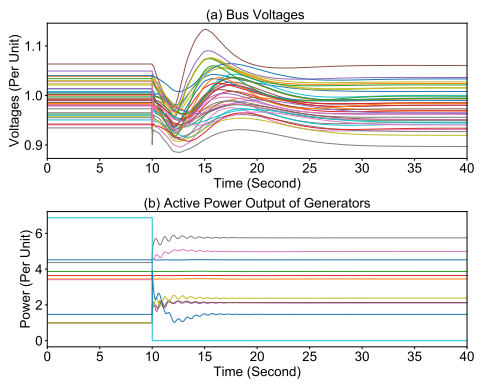


Fig. 8. System dynamic response under the FCUC dispatch and worst-case contingency during the scheduling period 24. (a) Bus voltages. (b) Generator active power outputs.

by the FCUC. The second column is the corresponding PSS/E verification. The third column is the PSS/E simulation of the ordinary UC dispatch. The term "NA" denotes instability cases. As we can see, ordinary UC dispatch is severely insecure as most dispatched conditions cannot withstand the worst-case contingency. Meanwhile, the FCUC significantly improve the stability and security with satisfactory prediction accuracy.

TABLE II

COMPARISON OF DEVIATED FREQUENCY NADIRS IN HZ FROM FCUC
PREDICTION AND PSS/E VERIFICATION

Period	Pred.	FCUC	UC	Period	Pred.	FCUC	UC
1	-0.75	-0.61	NA	13	-0.99	-0.99	NA
<b>2</b>	-0.90	-0.84	NA	14	-1.00	-0.98	NA
3	-1.00	-0.72	NA	15	-1.00	-1.04	NA
4	-1.00	-0.93	NA	16	-1.00	-0.99	NA
5	-0.94	-0.91	-1.66	17	-0.99	-0.99	NA
6	-0.98	NA	NA	18	-1.00	-0.98	NA
7	-0.98	NA	NA	19	-1.00	-0.98	NA
8	-0.99	-0.96	NA	20	-0.98	-0.99	NA
9	-1.00	-0.99	NA	<b>21</b>	-1.00	-1.00	NA
10	-0.89	-0.88	NA	22	-0.89	-0.87	NA
11	-1.00	-1.02	NA	23	-1.00	-0.75	NA
12	-0.98	-1.01	NA	24	-1.00	-0.76	NA

#### VII. CONCLUSIONS

The UC formulation without frequency response constraints will lead to insecure and unstable dynamic response under contingencies when the renewable penetration becomes high. The existing FCUC methods are either incapable to consider realistic models and corresponding stability or extremely difficult to solve. The paper presents a generic deep learning-based framework for FCUC, where two neural network models are constructed to represent the frequency nadir and stability

characteristics given a specific operating condition and a worst-case contingency. The proposed region-of-interest active sampling is effective in selecting power injection samples whose frequency nadirs are closer to the UFLS threshold. Such a dataset later proves to be beneficial for training accuracy improvement. The FCUC formulation can effectively schedule frequency secure generator commitments, which is verified using the PSS/E simulation.

#### REFERENCES

- J. Restrepo and F. Galiana, "Unit commitment with primary frequency regulation constraints," *IEEE Trans. Power Syst.*, vol. 20, no. 4, pp. 1836–1842, nov 2005.
- [2] Y. Y. Lee and R. Baldick, "A frequency-constrained stochastic economic dispatch model," *IEEE Trans. Power Syst.*, vol. 28, no. 3, pp. 2301–2312, 2013.
- [3] H. Chavez, R. Baldick, and S. Sharma, "Governor rate-constrained OPF for primary frequency control adequacy," *IEEE Trans. Power Syst.*, vol. 29, no. 3, pp. 1473–1480, 2014.
- [4] Y. Wen, W. Li, G. Huang, and X. Liu, "Frequency dynamics constrained unit commitment with battery energy storage," *IEEE Trans. Power Syst.*, vol. 31, no. 6, pp. 5115–5125, 2016.
- [5] F. Teng, V. Trovato, and G. Strbac, "Stochastic scheduling with inertiadependent fast frequency response requirements," *IEEE Trans. Power* Syst., vol. 31, no. 2, pp. 1557–1566, mar 2016.
- [6] V. Prakash et al., "Frequency response constrained modified interval scheduling under wind uncertainty," *IEEE Trans. Sustain. Energy*, vol. 9, no. 1, pp. 302–310, 2018.
- [7] L. Badesa, F. Teng, and G. Strbac, "Simultaneous scheduling of multiple frequency services in stochastic unit commitment," *IEEE Trans. Power* Syst., vol. 34, no. 5, pp. 3858–3868, 2019.
- [8] Z. Chu, U. Markovic, G. Hug, and F. Teng, "Towards optimal system scheduling with synthetic inertia provision from wind turbines," *IEEE Trans. Power Syst.*, vol. 35, no. 5, pp. 4056–4066, 2020.
- [9] P. M. Anderson and M. Mirheydar, "A low-order system frequency response model," *IEEE Trans. Power Syst.*, vol. 5, no. 3, pp. 720–729, 1990.
- [10] H. Ahmadi and H. Ghasemi, "Security-constrained unit commitment with linearized system frequency limit constraints," *IEEE Trans. Power Syst.*, vol. 29, no. 4, pp. 1536–1545, 2014.
- [11] A. Gholami and A. Sun, "Towards resilient operation of multimicrogrids: an MISOCP-based frequency-constrained approach," *IEEE Trans. Control Netw. Syst.*, vol. PP, no. c, p. 1, 2018.
- [12] A. Muzhikyan, T. Mezher, and A. M. Farid, "Power system enterprise control with inertial response procurement," *IEEE Trans. Power Syst.*, vol. 33, no. 4, pp. 3735–3744, 2018.
- [13] N. Nguyen, S. Almasabi, A. Bera, and J. Mitra, "Optimal power flow incorporating frequency security constraint," *IEEE Trans. Ind. Appl.*, vol. 55, no. 6, pp. 6508–6516, 2019.
- [14] Z. Zhang et al., "Modeling frequency dynamics in unit commitment with a high share of renewable energy," *IEEE Trans. Power Syst.*, vol. 8950, no. c, pp. 1–1, 2020.
- [15] G. Kou et al., "Impact of governor deadband on frequency response of the U.S. Eastern Interconnection," *IEEE Trans. Smart Grid*, vol. 7, no. 3, pp. 1368–1377, 2016.
- [16] I.-I. Avramidis, F. Capitanescu, S. Karagiannopoulos, and E. Vrettos, "A Novel Approximation of Security-Constrained Optimal Power Flow with Incorporation of Generator Frequency and Voltage Control Response," *IEEE Trans. Power Syst.*, vol. 8950, no. c, pp. 1–1, 2020.
- [17] X. Zhao et al., "Frequency stability constrained optimal power flow incorporating differential algebraic equations of governor dynamics," *IEEE Trans. Power Syst.*, vol. 8950, no. c, pp. 1–1, 2020.
- [18] R. Anderson, J. Huchette, C. Tjandraatmadja, and J. P. Vielma, "Strong mixed-integer programming formulations for trained neural networks," *Lect. Notes Comput. Sci. (including Subser. Lect. Notes Artif. Intell. Lect. Notes Bioinformatics)*, vol. 11480 LNCS, pp. 27–42, 2019.
- [19] Y. Zhang et al., "Approximating Trajectory Constraints with Machine Learning – Microgrid Islanding with Frequency Constraints," IEEE Trans. Power Syst., vol. Early Acce, pp. 1–8, 2020.
- [20] B. Settles, "Active learning literature survey," University of Wisconsin-Madison Department of Computer Sciences, Tech. Rep., 2009.
- [21] Siemens, PSS/E 33.5 Model Library, Siemens Industry, Inc., Schenectady, NY, USA, 2013.